



# Total organic carbon and total nitrogen removal and simultaneous electricity generation for nitrogen-containing wastewater based on the catalytic reactions of hydroxyl and chlorine radicals



Yan Zhang<sup>a</sup>, Jinhua Li<sup>a</sup>, Jing Bai<sup>a,\*</sup>, Xiaoyan Li<sup>a</sup>, Zhaoxi Shen<sup>a</sup>, Ligang Xia<sup>a</sup>, Shuai Chen<sup>a</sup>, Qunjie Xu<sup>b,c</sup>, Baoxue Zhou<sup>a,c,d,\*</sup>

<sup>a</sup> School of Environmental Science and Engineering, Shanghai Jiao Tong University, No. 800, Dongchuan Rd, Shanghai 200240, PR China

<sup>b</sup> College of Environmental and Chemical Engineering, Shanghai University of Electric Power, No.2588 Changyang Road, Shanghai, 200090, PR China

<sup>c</sup> Shanghai Institute of Pollution Control and Ecological Security, Shanghai 200092, PR China

<sup>d</sup> Key Laboratory of Thin Film and Microfabrication Technology, Ministry of Education, Shanghai 200240, PR China

## ARTICLE INFO

### Keywords:

Total nitrogen  
Nitrogen-Containing organic wastewater  
Catalytic reactions of hydroxyl and chlorine radicals  
Wastewater fuel cell  
Self-biased

## ABSTRACT

The treatment of nitrogen-containing organic wastewater is a difficult problem because organic and nitrogen contents are hard to remove simultaneously for the common sewage disposal technologies. Here we propose a new method to efficiently remove total organic carbon and total nitrogen and generate electricity simultaneously for this wastewater. The key idea of design is that organics and ammonia nitrogen is converted into CO<sub>2</sub> and N<sub>2</sub> by catalytic reacting with hydroxyl and chlorine radicals, respectively, while generating electricity concurrently in a self-biased wastewater fuel cell. Nitrate-N (including original or generated) was reduced on Pd/Cu modified Ni foam electrode with high selectivity toward N<sub>2</sub>, realizing the completely removal of total nitrogen from the water. Moreover, self-bias voltage was generated by employing WO<sub>3</sub> nanoplate array electrodes and silicon photovoltaic cells as a hybrid photoanode to enhance the charge separation. This system was also successful in extending the light harvest. A series of experiments were performed with nitrate-N (ammonium-N) and phenol and the results indicated the removal efficiency of nitrate-N (ammonium-N) was 98.7% (91.5%) in 90 min and total nitrogen was efficiently transformed to N<sub>2</sub> with extending time to 120 min. The system also showed a superior performance for phenol degradation (99.1% in 90 min). Combined with the analysis of ESR and free radical capture experiment, it was concluded that chlorine radical played an important role in the phenol and ammonia-N oxidation. In addition, maximum power density output of the system reached 1.23 mW cm<sup>-2</sup>. This study offers a self-sustaining approach for simultaneous nitrogen-containing organic wastewater treatment and electricity production.

## 1. Introduction

The treatment of nitrogen-containing organic wastewater discharged from industries or agriculture is a challenge for environmental researchers. This effluent contains large amount of organic compounds and inorganic nitrogen (nitrate-N and ammonium-N), which are difficult to deal with simultaneously and may cause adverse effects on human health and ecosystem [1,2]. Biological treatment is an economical way to decompose organics, while its performance is greatly affected by the C/N ratio. When C/N ration was lower or higher C/Ns (3 and 30), nitrate-N cannot be effectively removed [3]. To improve the treatment effect, anaerobic-anoxic-oxic process [4] and extending the

hydraulic retention time [5] are applied, leading to more consumption of energy. Other methods, for example, ion exchange [6,7], chemical process [8,9] and electrochemical processes [10] are constrained by the low efficiency to transform inorganic nitrogen into nitrogen gas. Wang et al. treated ammonia-N using the photoelectrochemical technique, about 49.1% of which was converted to nitrate-N and could not be eliminated [11]. Moreover, both the oxidation of organics and ammonia-N is the exothermic process, it is meaningful to recover chemical energy in the process of wastewater purification [12].

Recently, microbial fuel cell (MFC) [13–15] and photocatalytic fuel cell (PFC) [16–18] realize the concept of generating electricity in the process of degrading organics by microbial community and

\* Corresponding authors at: School of Environmental Science and Engineering, Shanghai Jiao Tong University, No. 800, Dongchuan Rd, Shanghai 200240, PR China.

E-mail addresses: [bai\\_jing@sjtu.edu.cn](mailto:bai_jing@sjtu.edu.cn) (J. Bai), [zhoubaoxue@sjtu.edu.cn](mailto:zhoubaoxue@sjtu.edu.cn) (B. Zhou).

semiconductor photoanode [19–22], respectively. Compared with MFC, PFC has drawn more attention due to its fast electron transfer and simple operation. In addition, both ammonium-N and nitrate-N with high concentration would inhibit the growth of microorganisms in MFC [23]. However, nitrate is reduced to ammonia in most cases, while ammonia tends to be oxidized to nitrate in PFC system, which leads to low removal of total nitrogen (TN). Therefore, development of an effective approach that can simultaneously remove total organic carbon (TOC) and convert nitrogen elements to N<sub>2</sub> still is a challenge.

Herein, we propose, for the first time, a new method to effectively remove TOC and TN and generate electricity simultaneously for nitrogen-containing organic wastewater based on the catalytic reactions of hydroxyl and chlorine radicals. Compared with common PFC, this system has the following three features. First, ammonia-N is converted into N<sub>2</sub> by chlorine radicals, while organic matter is mineralized into CO<sub>2</sub> by hydroxyl radical, recycling chemical energy in the form of electricity. The introduction of chloride ion will expand the radical reaction from the anode surface to the whole solution, forming a sustainable radical chain reaction. Under illumination, chlorine radicals are generated on oxidation of Cl<sup>−</sup> by photoholes, which has high oxidation potential and reacts with electro-rich moieties more rapidly than ·OH [24]. With sufficient chlorine radicals, NH<sub>4</sub><sup>+</sup>-N is trapped and oxidized to N<sub>2</sub> through a redox reaction, realizing the catalytic cycle of chlorine. Meanwhile, organics are transformed into CO<sub>2</sub> and small molecule carboxylic acids [25]. Secondly, a cathode with high activity and selectivity was used to increase the conversion efficiency of inorganic nitrogen to N<sub>2</sub>, eliminating the byproducts such as nitrite and nitrate during ammonium-N oxidation. Various group metals [5,10] have been investigated and Pd-Cu is accepted as a promising combination for catalytic reduction of nitrate to N<sub>2</sub> [26]. Unfortunately, the nitrate reduction is slow because of its negative charge, which limits the adsorption on cathode surface. Ni foam (NF) is of great potential as the support for Pd-Cu alloy due to its porous structure, low cost and high conductivity [27]. Pd-Cu alloy modified Ni foam electrode (Pd-Cu/NF) can enhance the adsorption of nitrate on cathode surface by its characteristics of capacitor. After adsorption on cathode, NO<sub>3</sub><sup>−</sup> was reduced to NO<sub>2</sub><sup>−</sup> on the Cu site and then NO<sub>2</sub><sup>−</sup> reduced to N<sub>2</sub> on the Pd site, realizing nitrogen completely removal from water.

Third, to enhance the charge separation, a hybrid photoanode was designed based on WO<sub>3</sub> photoanode in series with a rear silicon photovoltaic cell (WO<sub>3</sub>/Si PVC) without applied bias. By using two light absorbing junctions with different bandgaps, the hybrid photoanode can achieve extended light harvesting than those on a single junction. In addition, the commercial silicon PVC pack was chosen here because it is non-toxic, cheap, and scalable [28]. Although the device has been reported for photo-driven water splitting [29], there is no study about it in environmental pollution control. Moreover, the hybrid photoanode can generate sufficient voltage to overcome the thermodynamic and kinetic barriers for nitrate reduction [30].

Based on the capability to mineralize organics into CO<sub>2</sub> and convert nitrogen into N<sub>2</sub>, a wastewater fuel cell (WFC) paired with WO<sub>3</sub>/Si PVC hybrid photoanode and Pd-Cu/NF cathode was constructed for nitrogen-containing organic wastewater treatment and simultaneous electricity generation, which were performed under bias-free conditions. Visible light response WO<sub>3</sub> [31] and a commercial silicon PVC pack were used as the front and rear photoanodes, respectively. Through this system, Pd-Cu/NF electrode was prepared by electro-deposition method and total nitrogen and phenol removal were evaluated in view of the effects of various operation parameters and the final products. Overall, the proposed self-biased WFC provides a sustainable way to degrade organic wastewater containing nitrogen and generate electricity simultaneously for practical applications.

## 2. Experimental

### 2.1. Chemicals and materials

Fluorine-doped tin oxide (FTO) glass (13 Ω cm<sup>−1</sup>) was purchased from Nippon Sheet Glass Co., Ltd. Ni foam was obtained from Kunshan Jiayisheng Electronics Co., Ltd. All chemicals used were of analytical reagents grade. Sodium nitrate, ammonium sulfate and palladium chloride were purchased from Sinopharm Chemical Reagent Co., Ltd.

### 2.2. Preparation of Pd-Cu/NF cathode

Ni foam was cut into 2 × 4 cm<sup>2</sup> pieces, and then ultrasonically cleaned in acetone, 0.5 M H<sub>2</sub>SO<sub>4</sub> solution and distilled water, respectively. The Pd-Cu/NF was synthesized by electrodeposition under potentiostatic control [32]. It was performed in a three electrode system where Ni foam served as working electrode, the platinum mesh as counter electrode and a saturated calomel electrode (SCE) as reference electrode. Specifically, electrolyte was composed of 2 mM PdCl<sub>2</sub>, 4 mM CuSO<sub>4</sub> and 0.01 M HCl and the preparation was conducted at −1.0 V vs. SCE for 30 min. After that, the prepared electrode was washed with deionized water and dried in air.

### 2.3. Fabrication of the WO<sub>3</sub>/Si PVC photoanode

The WO<sub>3</sub> nanoplate array (WO<sub>3</sub> NPs) was prepared previously described [33], and detailed procedure was shown in Supporting Information. Photographs of Si PVC, WO<sub>3</sub> photoanode and WO<sub>3</sub>/Si PVC hybrid electrode were shown in Fig. S1. A commercial Si PVC pack was used as the rear photoanode and it was composed of eight single-junction cells (0.5 × 4 cm<sup>2</sup>). The silicon PVC cells were attached to the printed circuit board side by side, and then were connected in series via tabbing wire and Ag epoxy. This structure was encapsulated by transparent acrylic laminating tape that can provide protection from aqueous media. The silicon PVC was bonded to the back of the WO<sub>3</sub> and sealed with silicone rubber to form a hybrid photoanode. The WO<sub>3</sub> electrode was connected to the positive pole of Si PVC and electrical contact was made by copper wire.

### 2.4. Experimental setup

The degradation of phenol and nitrate-N (ammonium-N) was processed in a single chamber quartz reactor under simulated solar light (100 mW cm<sup>−2</sup>) using a 350 W Xe lamp (Perfect, China). 40 mL of synthetic wastewater containing 30 mg L<sup>−1</sup> nitrate-N (20 mg L<sup>−1</sup> ammonium-N), 20 mg L<sup>−1</sup> phenol, 0.05 mol L<sup>−1</sup> Na<sub>2</sub>SO<sub>4</sub> and 0.05 M NaCl was treated at pH 5.0. The initial solution pH was adjusted by NaOH or H<sub>2</sub>SO<sub>4</sub> (0.1 M). The Pd-Cu/NF (working area of 6 cm<sup>2</sup>) worked as the cathode, and WO<sub>3</sub>/Si PVC acted as the photoanode with the same area (Fig.S2), while the distance between the two electrodes is 1.5 cm. An electrochemical workstation was used to monitor the current.

### 2.5. Analytical methods

The morphologies of the prepared electrodes were investigated by scanning electron microscope (SEM, Zeiss SUPRA55-VP) with an energy-dispersive X-ray (EDX) spectrometer. The X-ray diffraction (XRD) measurements were performed on a Rigaku D-Max B. The composition of Pd-Cu/NF electrode was analyzed with an Omicron EA125 X-ray photoelectron spectroscopy (XPS). The UV-Vis absorption spectra of the samples were recorded on a photospectrometer equipped with an integrating sphere (TU-1901, Pggeneral, China). Electron spin resonance (ESR) spectra was obtained on a Bruker ESP 300E Spectrometer [34]. The concentration of free chlorine was determined by the DPD/FAS titration method [35].

Linear sweep voltammetry (LSV) was operated at scan rate of 50 mV

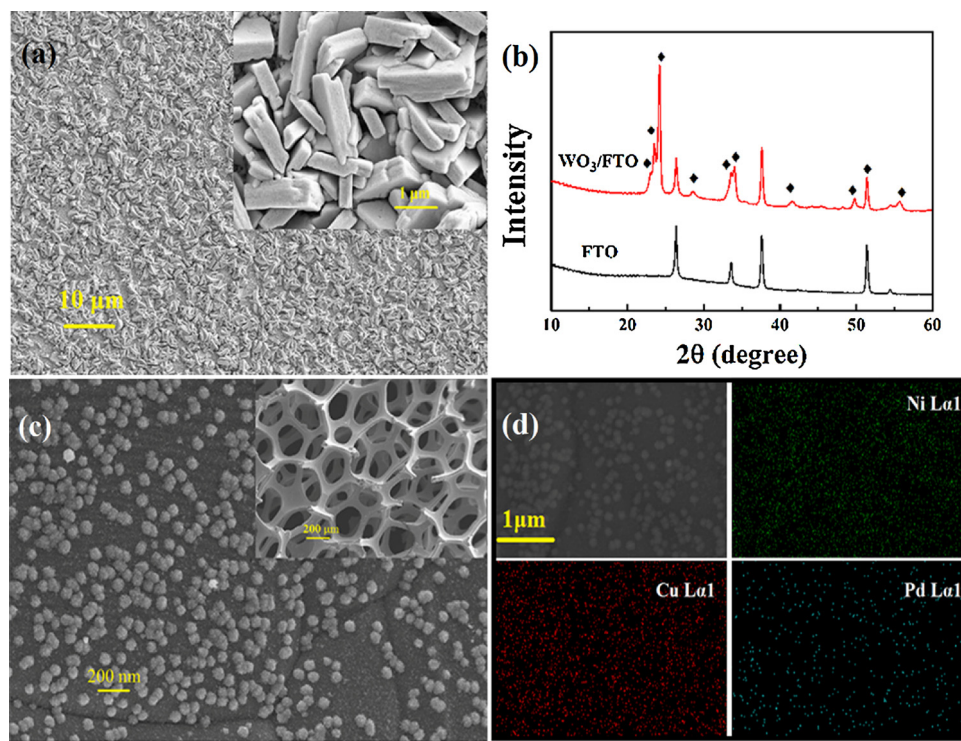


**Fig. 1.** (a) The top view SEM images of WO<sub>3</sub> photoanode. (b) XRD patterns of WO<sub>3</sub> photoanode (c) SEM images of the Pd-Cu/NF cathode. (d) EDS elemental mapping of Pd-Cu/NF cathode.

s<sup>-1</sup> between –1.8 and 0.2 V vs. SCE. The current-voltage characteristics of WFC system were measured by LSV in a two-electrode system and the detail was in the Supporting Information. Phenol was determined by high-pressure liquid chromatography (LC-20AT, Shimadzu, Japan) equipped with a C-18 column and detected at 254 nm using a UV detector. The measurements of carboxylic acids were performed using LC-20AT with an AQ-C18 chromatographic column and a UV detector at 210 nm. Nitrate-N and nitrite-N were determined using an ion chromatograph (Dionex, USA), and ammonia-N concentration was measured by Nessler reagent method, using a 752 N UV-vis spectrophotometer at 420 nm. The TOC removal was determined by a multi 3100 TOC/TN analyzer (Analytikjena, Germany).

### 3. Results and discussion

#### 3.1. Characterization of the electrodes

**Fig.1a** showed the SEM images of WO<sub>3</sub> NPs grown on the FTO substrate. It showed WO<sub>3</sub> film appeared to be plate-like morphology uniformly over the substrate. **Fig.1b** showed the XRD patterns of WO<sub>3</sub> NPs and the main diffraction peaks were observed at 23.3°, 23.8°, and 24.6°, which correspond to reference pattern for monoclinic WO<sub>3</sub> (JCPDS no. 43-1035) [27]. The photocurrent-potential plot of the WO<sub>3</sub> was measured using chopped light in **Fig.S3**. It showed that the photocurrent density was 0.55 mA cm<sup>-2</sup> at 0.6 V vs SCE, which indicated WO<sub>3</sub> NPs had a good photocatalytic capacity.

**Fig.1c** showed the SEM image of Pd–Cu/NF and the illustration was pure NF. The bare NF had a 3D porous structure with abundant superficial wrinkles [36]. After deposition, the surface of NF became rough. It showed that the electrodeposited Pd–Cu alloy with spheroidal shape was uniformly dispersed on NF, though some agglomerations. The crystal size of Pd–Cu alloy was about 100 nm, and the arrangement could increase the surface area. Moreover, the EDS elemental mapping (**Fig.1d**) also confirmed that these elements were distributed on NF. The XRD pattern of Pd–Cu/NF was shown in **Fig.S4a**. A diffraction peak at 40.1° corresponded to the Pd. However, the peak for Cu was not

observed and the formation of Cu<sub>3</sub>Pd phase may be the reason [37].

To identify the valence states of Pd and Cu on NF cathode, XPS measurement was carried out and the spectrum (**Fig. S4b**) revealed the existence of Pd and Cu in the electrode. As shown in **Fig. S5a**, the binding energies at around 340.6 and 335.3 eV of the Pd 3d peaks indicate the existence of Pd<sup>0</sup> [38]. **Fig. S5b** presented narrow scans of Cu 2p and three chemical states can be detected. The fitting peaks at 931.8, 933.4, and 934.9 eV correspond to Cu<sup>0</sup>, Cu<sup>I</sup>, and Cu<sup>II</sup>, respectively [39]. The presence of Cu<sup>I</sup> and Cu<sup>II</sup> in the cathode before reaction may be due to the oxidation of Cu<sup>0</sup> by atmospheric oxygen.

#### 3.2. Nitrate-N reduction on Pd–Cu/NF cathode

Control experiments were conducted to compare the removal of nitrate-N by different electrodes. Pt is commonly used cathode in photoelectrochemical system, while NF is the substrate material for Pd–Cu/NF. **Fig.2a** showed that Pd–Cu/NF electrode had the best performance and 29.6 mg L<sup>-1</sup> of nitrate-N was removed in 90 min. When NF electrode was used, 8.3 mg L<sup>-1</sup> of nitrate-N was removed. Only 6.4 mg L<sup>-1</sup> of nitrate-N was removed for the Pt cathode. This is most likely due to the enhanced H<sub>2</sub> evolution on Pt electrode, which inhibits the reduction of nitrate. In addition, the nitrate reduction process was found to obey pseudo-first-order kinetics (**Fig.2b**). The rate constant for Pt, NF and Pd–Cu/NF electrode was calculated to be 0.0026, 0.003 and 0.036 min<sup>-1</sup>, respectfully, which suggested that Pd–Cu/NF electrode exhibited the highest nitrate conversion.

To evaluate the reduction characteristics of nitrate at Pd–Cu/NF cathode, linear sweep voltammetry was measured. As presented in **Fig.3a**, the LSV of NF showed an obvious current rise at -1.0 V vs SCE in chloride solution, which was water electrolysis to produce H<sub>2</sub> [40]. After adding nitrate, an increased current occurred at -1.2 V vs SCE, attributing to the reduction of nitrate. In all cases, Pd–Cu/NF showed a higher current under same scanning operation (**Fig.3b**), which indicated it exhibited better nitrate reduction ability. The peak at -0.9 V vs SCE was due to the reduction of Cu<sub>2</sub>O to Cu. Interestingly, a current peak occurred at -0.6 V vs SCE on Pd–Cu/NF and it was due to the

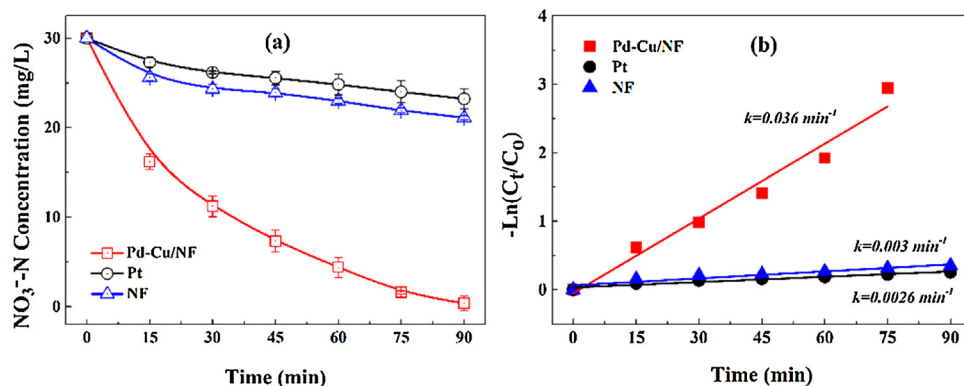


**Fig. 2.** (a)  $\text{NO}_3^-$ -N removal and (b) the plots of  $\ln(C_t/C_0)$  versus time for the  $\text{NO}_3^-$ -N degradation at different cathodes. Condition: pH = 5, NaCl 0.05 M, 30 mg L<sup>-1</sup>  $\text{NO}_3^-$ -N.

adsorption of nitrate [41]. However, no corresponding peak was observed on NF cathode and it indicated that nitrate was easily captured by Pd-Cu/NF cathode. This may be because Pd-Cu/NF had the properties of capacitors, thereby promoting the adsorption of nitrate. Since the affinity of Pd for hydrogen adsorption is documented [42], an electric double layer is formed on the surface of the cathode, which can reduce the electrostatic repulsion between the nitrate and the cathode, and promotes the nitrate to obtain electrons. Moreover, the Cu modified cathode has good ability of adsorption for  $\text{NO}_3^-$  or  $\text{NO}_2^-$ , because the two molecules can be adsorbed on the Cu (100) surface via two oxygen atoms [43]. Moreover, the 3D structure of Pd-Cu/NF electrode can provide efficient penetration pathways, fast diffusion channels and high surface areas for ion accommodation [44].

### 3.3. Major factors influencing nitrogen and phenol removal

#### 3.3.1. Effect of pH

We investigated the influence of pH values on the nitrate reduction and the results were presented in Fig. 4. About 29.6 mg L<sup>-1</sup> of nitrate-N was removed at pH 5, while pH 3.0 solution yielded 25.8 mg L<sup>-1</sup> nitrate-N degradation. The decrease in conversion rate was due to the competition of hydrogen ion with nitrate. Lower nitrate-N removal efficiency was also observed when pH at below 3 because of the strong inhibition by hydrogen evolution. Along with increasing the pH value, nitrate degradation decreased from 29.6 at pH 5 to 26.6 mg L<sup>-1</sup> at pH 7.0, then considerably decreased to 23.4 mg L<sup>-1</sup> at pH 9. The degradation of nitrate-N decreased with the increase of pH and it was attributed to the  $\text{WO}_3$  photoanode, which is not stable under strong alkali condition. Moreover, nitrate-N reduction may be carried out in the presence of hydrogen as a reducing agent. We therefore investigated the pH variation during the experiments and found the pH of solution increased gradually along with time (Fig.S6), which was indicative of

the hydrogen production during nitrate reduction. Cyclic voltammograms curves of Pd-Cu/NF electrode were measured and the highest reduction peak was obtained in the solution of pH = 5 (Fig.S7), confirming the reduction of nitrate was improved. In addition, nitrite-N was not detected during the experiment. We also studied the effect of initial pH on the degradation efficiency of phenol. Fig. 4b illustrated phenol could be effectively degraded at various pH values although its removal efficiency still depended on the initial pH. Along with increasing the pH, the phenol degradation decreased from 99.1% at pH 3.0 to 95.3% at pH = 7, then decreased to 90.5% at pH 9.0.

#### 3.3.2. Effect of Si PVC

Using commercial Si PVC, the  $\text{WO}_3$ /Si PVC hybrid photoanode was fabricated, and its bias-free phenol and nitrate-N degradation performance were evaluated. As shown in Fig. 5a, the  $\text{WO}_3$  photoanode and Si PVC were assembled in series, where  $\text{WO}_3$  photoanode absorbed sunlight at wavelengths below 500 nm and the rest of solar light above 500 nm was absorbed by Si PVC. Hence, longer-wavelength of incident light remains available for the Si PVC placed behind the  $\text{WO}_3$ , which can generate sufficient photovoltage to overcome the thermodynamics for reducing  $\text{NO}_3^-$  to  $\text{N}_2$  at Pd-Cu/NF cathode. Next, the light absorption of Si PVC and transmittance of  $\text{WO}_3$  photoanode were measured. Fig. 5b showed that higher than 40% light in the range of 500 to 700 nm can transmit to  $\text{WO}_3$  photoanode and the Si PVC had intensive absorption in the longer wavelength region (500 to 700 nm), which meant that  $\text{WO}_3$  photoanode and Si PVC had complementary absorption of sun light. It suggested that the exploitation of solar light can significantly enhanced in WFC system. In this system, output voltage of PVC is important because it affects the current density. It's known that a silicon PVC cell produces a voltage of 0.5–0.6 V under standard conditions [30], and the commercial silicon PVC pack that several cells connected electrically in series was used to create sufficient potential.

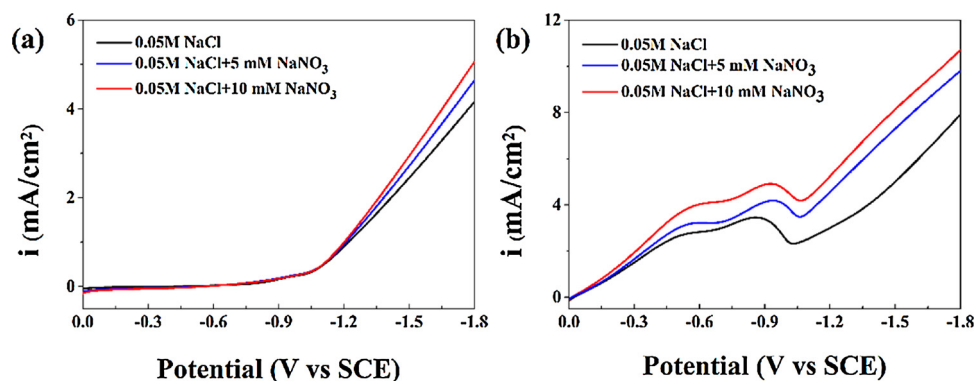


**Fig. 3.** Linear sweep voltammetry curves of  $\text{NO}_3^-$  in  $\text{Cl}^-$  solution at pure NF cathode (a) and Pd-Cu/NF cathode (b). Scan rate: 50 mV S<sup>-1</sup>, pH = 5.

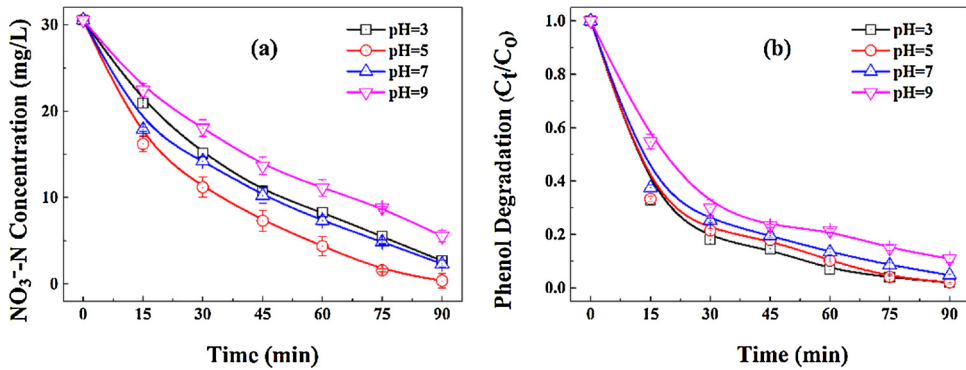


Fig. 4. Effect of pH on (a)  $\text{NO}_3^-$ -N removal and (b) phenol degradation. Condition:  $\text{NaCl}$  0.05 M,  $30 \text{ mg L}^{-1}$   $\text{NO}_3^-$ -N,  $20 \text{ mg L}^{-1}$  phenol.

Since the number of solar panels in series was 2, 4, 6 and 8, Si PVC electrodes were marked as PVC-2, PVC-4, PVC-6 and PVC-8, respectively. In Fig. 5c, nitrate-N was not degraded in the WFC system using  $\text{WO}_3$ /Si PVC-2 as the anode within 90 min. We found that nitrate reduction significantly increased with improving the serial numbers from 2 to 8. As shown in Fig. S8, the photocurrent density increased from 0.7 to  $4.4 \text{ mA cm}^{-2}$  when the number of PVC increased from 2 to 8. This may be because the reduction of nitrate occurs at a certain current density. Similarly, the removal efficiency of total nitrogen in PVC-2, PVC-4, PVC-6 and PVC-8 system was 0.65, 8.99, 18.58 and  $29.2 \text{ mg L}^{-1}$ , respectively (Fig. S9). In comparison, minimal ammonium-N was detected in the process by different anodes. High output voltage was benefit for the nitrogen removal. The trend in the degradation of phenol was consistent with that of nitrate reduction, and the highest degradation efficiency was obtained when 8 cells in series (Fig. 5d). Therefore, a Si PVC pack with 8 cells in series was used in the following study.

### 3.3.3. Effect of $\text{Cl}^-$ concentration

The chlorine ion is also crucial for the nitrate-N degradation, which can remove total nitrogen completely from the water. Fig. 6a illustrated

nitrate-N removal efficiency at different chlorine concentrations. The removal efficiency of nitrate-N showed a slight increase in the presence of chloride. Even without chloride, the conversion of nitrate was about  $28.3 \text{ mg L}^{-1}$  after 90 min treatment. In contrast, chloride had great influence on ammonium-N generation [45]. As displayed in Fig. 6b, the  $\text{NH}_4^+$ -N concentration sharply decreased by chloride concentration increasing. In the absence of chlorine, we found that  $9.63 \text{ mg L}^{-1}$  ammonium-N remained in solution, while the remaining was  $2.61 \text{ mg L}^{-1}$  when 0.025 M of chlorine was present. With the increase of chloride concentration to 0.05 or more, nearly no ammonium-N was detected. The ammonium-N could be converted to  $\text{N}_2$  due to the formation of  $\text{Cl}\cdot$ , which led to an improvement in TN removal. To test this conjecture, we measured the TN removal in different chloride concentrations (Fig. 6c). Along with increasing chloride concentration from 0 to 0.05 M, TN removal increased from 65.8% to 96.3%. When 0.075 M chloride was used, no obvious improvement in TN removal was observed. In addition, phenol degradation was significantly enhanced by increasing chlorine concentration to 0.05 M (Fig. 6d). Phenol degradation efficiency was only 70% in the absence of NaCl and it was accelerated (99%) in the presence of 0.05 M NaCl. It was previously reported that reaction rate of  $\text{Cl}\cdot$  with organic molecules is similar to that of  $\cdot\text{OH}$

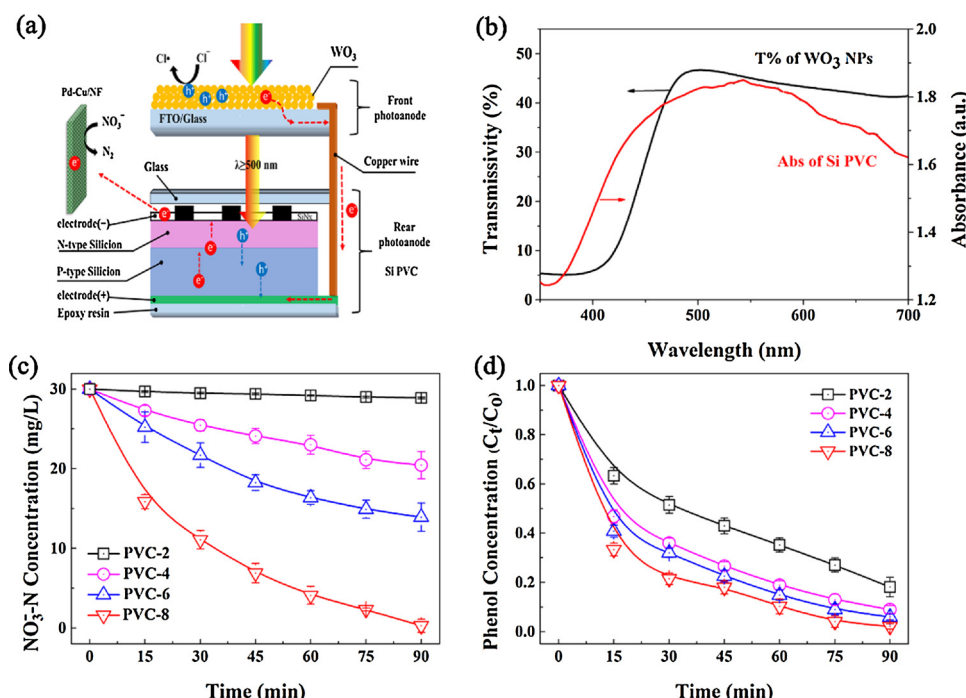
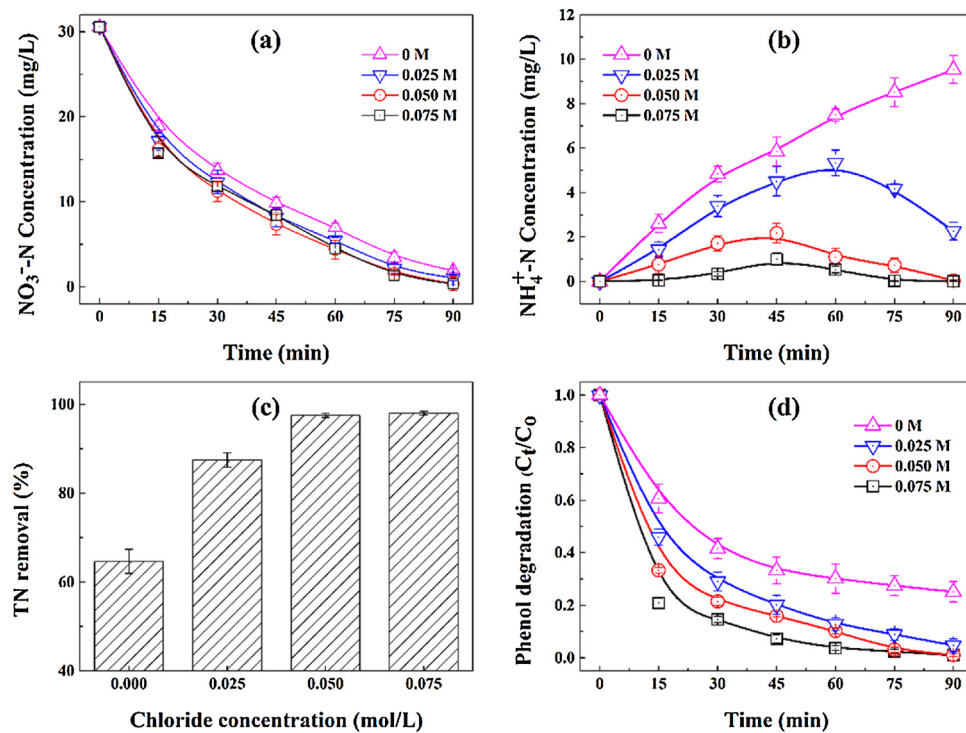


Fig. 5. (a) Schematic drawing of the  $\text{WO}_3$  photoanode and silicon photovoltaic cell (Si PVC). (b) The light transmissivity of the  $\text{WO}_3$  and the light absorbance of Si PVC. Effect of the junction number on (c)  $\text{NO}_3^-$ -N removal and (d) phenol degradation. Condition: pH = 5,  $\text{NaCl}$  0.05 M,  $30 \text{ mg L}^{-1}$   $\text{NO}_3^-$ -N,  $20 \text{ mg L}^{-1}$  phenol.



**Fig. 6.** Effect of chlorine concentration on (a)  $\text{NO}_3^-$ -N removal, (b)  $\text{NH}_4^+$ -N generation, (c) total nitrogen removal and (d) phenol degradation. Condition: NaCl 0.05 M, pH = 5, 30 mg L<sup>-1</sup>  $\text{NO}_3^-$ -N and 20 mg L<sup>-1</sup> phenol.

[46]. This may be due to the enhanced chorine evolution, which generates reactive chlorine species to achieve more phenol removal.

It is well-known that chlorine ion can be oxidized on anode to form free chlorine, which is also a potent oxidant. We thus measured the concentration of free chlorine in the system. Obviously, the concentration of free chlorine gradually increased to 38.1 mg L<sup>-1</sup> during  $\text{NH}_4^+$ -N and phenol degradation (Fig. 7a). For acidic condition, free chlorine existed in the form of hypochloric acid and hypochloric acid participated in the  $\text{NH}_4^+$ -N and phenol degradation. To confirm the

role of free radicals in organics degradation, benzoic acid (BA) was chosen as a probe agent because it reacts with  $\cdot\text{OH}$ ,  $\text{Cl}\cdot$  or  $\text{Cl}_2\cdot^-$ , but does not react with free chlorine [47]. In Fig. 7b, BA degradation solution was slow in the  $\text{Na}_2\text{SO}_4$  solution. However, BA degradation efficiencies increased in the presence of 0.05 and 0.07 M NaCl, which implied that more radicals were generated. To distinguish the contributions of the  $\cdot\text{OH}$  and  $\cdot\text{Cl}$ , we performed the experiments by using different radical inhibitors. Tert-butyl alcohol (TBA) can react with both  $\cdot\text{OH}$  and  $\cdot\text{Cl}$ , while nitrobenzene (NB) only reacts with  $\cdot\text{OH}$  [48].

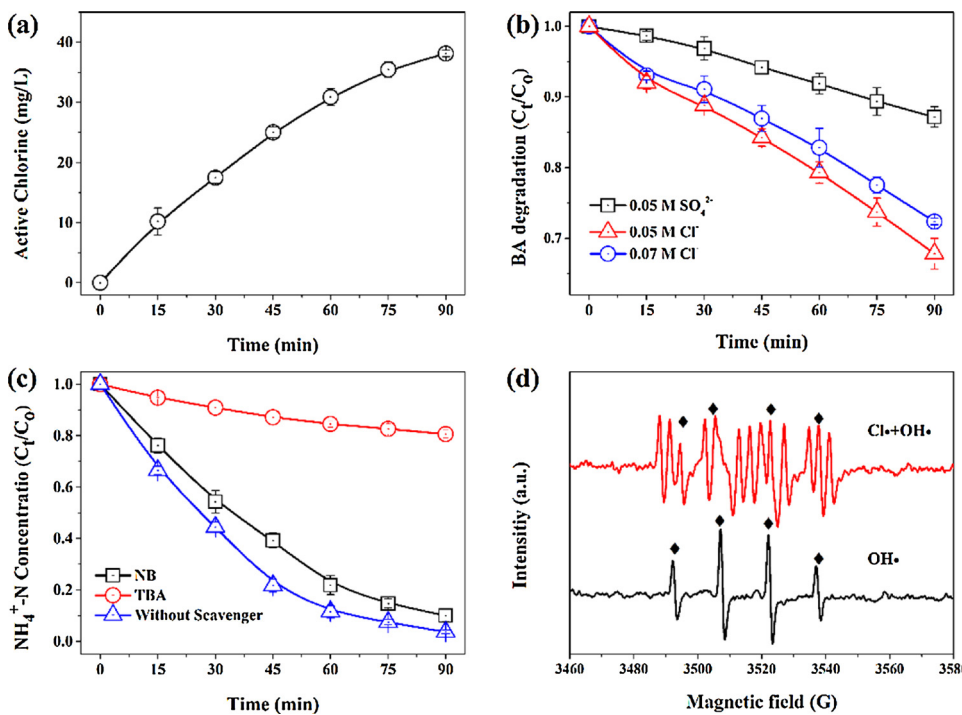


**Fig. 7.** (a) Variation of free chlorine concentration during the reaction. (b) Benzoic acid degradation (30 mg L<sup>-1</sup>) with  $\text{WO}_3/\text{Si}$  PVC under variable  $\text{Cl}^-$  concentration. (c)  $\text{NH}_4^+$ -N degradation efficiency by adding with different scavengers. (d) ESR spectra in the self-biased WFC system. Condition: NaCl 0.05 M, pH = 5 and 20 mg L<sup>-1</sup>  $\text{NH}_4^+$ -N.

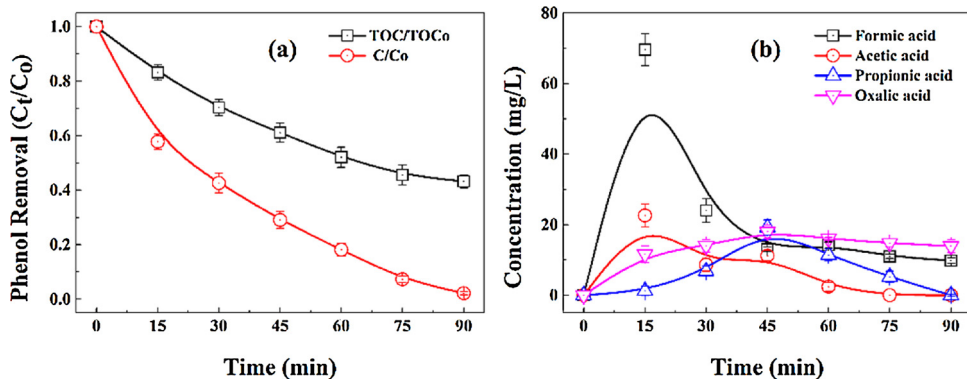


Fig. 8. (a) the changes of phenol and TOC removal efficiency with reaction time. (b) Evolution of the concentration of intermediates. The initial conditions: NaCl 0.05 M, pH = 5, nitrate-N 30 mg L<sup>-1</sup> and phenol 20 mg L<sup>-1</sup>.

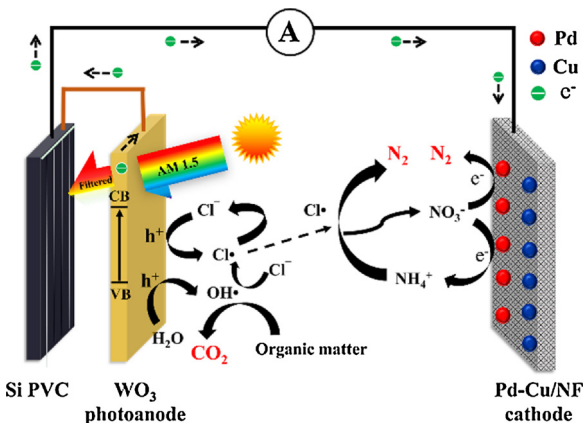


Fig. 9. Schematic illustration of organic wastewater containing nitrogen removal mechanism in the self-biased waster fuel cell system (AM 1.5 G sunlight at 100 mW cm<sup>-2</sup> intensity).

Fig. 7c showed that the degradation of ammonium-N sharply decreased with addition of TBA, implying that OH<sup>·</sup> and Cl<sup>·</sup> were both involved in ammonium-N oxidation. Only 10% of ammonium-N degradation was inhibited in the presence of NB, which suggested that Cl<sup>·</sup> played a major role. Then, ESR analysis was used to verify the short-lived radical species. As depicted in Fig. 7d, only a 4-fold characteristic peak with 1:2:2:1 intensity was detected when there is no chloride ion in the solution [49], indicating the generation of OH<sup>·</sup>. Furthermore, an eleven-fold characteristic peak was obtained after the addition of Cl<sup>-</sup>. According to previous reports, the seven-fold ESR spectrum corresponds to ·Cl/DMPO complex [50], indicating the generation of ·Cl in the process.

TOC removal was measured as an indicator for the mineralization of phenol. Fig. 8a showed that the maximum TOC removal of 56.2% was achieved at 90 min, indicating that a residual amount of organics remained in solution. Since the aromatics could be decomposed into small molecule carboxylic acids, we thus detected the intermediate products by liquid chromatogram. Fig. 8b showed that formic and oxalic acids were accumulated in the solution. The concentration of formic acid increased to 69.6 mg L<sup>-1</sup> at 15 min and considerably decreased to 9.8 mg L<sup>-1</sup> (Theoretical calculated TOC 2.56 mg L<sup>-1</sup>) at 90 min. In addition, oxalic acid gradually accumulated, up to 13.9 mg L<sup>-1</sup> (Theoretical calculated TOC 3.71 mg L<sup>-1</sup>) at 90 min. Therefore, small molecular organic acids (oxalic and formic acid) were associated with the remaining TOC in solution.

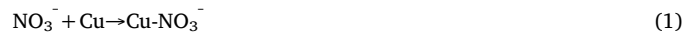
### 3.3.4. The effect of phenol concentration for nitrogen removal

The concentrations of nitrate and ammonium in the system were determined at regular time intervals. The nitrate degradation was little

affected by the phenol concentration (Fig.S10a), while ammonium generation was more sensitive to the phenol (Fig.S10b). When phenol concentration was below 20 mg L<sup>-1</sup>, NH<sub>4</sub><sup>+</sup>-N can be removed completely; However, when phenol concentration was 30 mg L<sup>-1</sup>, there was 1.8 mg L<sup>-1</sup> of NH<sub>4</sub><sup>+</sup>-N left after 90 min operations. If prolonging reaction time to 120 min, NH<sub>4</sub><sup>+</sup>-N could be eliminated. This phenomenon may be attributed to the competition between NH<sub>4</sub><sup>+</sup> and phenol. To confirm the feasibility of WFC system for treatment of wastewater with NH<sub>4</sub><sup>+</sup>-N, we investigated the degradation of 20 mg L<sup>-1</sup> NH<sub>4</sub><sup>+</sup>-N in the solution containing 20 mg L<sup>-1</sup> phenol. As shown in Fig.S11, we found that 91.5% of NH<sub>4</sub><sup>+</sup>-N was degraded within 90 min, and the NH<sub>4</sub><sup>+</sup>-N removal efficiency increased to 99% with prolonging the reaction time to 120 min. During the catalytic NH<sub>4</sub><sup>+</sup>-N oxidation, NO<sub>3</sub><sup>-</sup>-N increased slightly to 5.35 mg L<sup>-1</sup> after 30 min, but decreased to zero at 120 min. In contrast, the NO<sub>2</sub><sup>-</sup>-N concentration was still low during 120 min reactions.

### 3.4. Mechanism of NO<sub>3</sub><sup>-</sup>-N reduction on cathode

Based on the above experiments, a possible mechanism for treating organic wastewater containing nitrogen in the self-biased WFC system was shown in Fig. 9. In this system, the nitrogen removal was achieved through a cycle reaction and NO<sub>3</sub><sup>-</sup>-N was reduced in cathode. The Pd-Cu/NF can quickly absorb nitrate because of the characters of capacitor (Eq. (1)). After adsorption on the cathode surface, nitrate was reduced to nitrite on the Cu sites and then converted to N<sub>2</sub> on the Pd sites. To verify this hypothesis, the compositions of Pd-Cu/NF cathode before and after reaction were analyzed by XPS for investigating possible surface reactions (Fig.10). The surface composition of Cu<sup>1</sup> increased after the reaction (Fig.10a), while that of Cu<sup>0</sup> decreased. This result indicated that Cu<sup>0</sup> was oxidized to Cu<sup>1</sup> during the nitrate reduction; it also implied nitrate was first adsorbed on the surface of Cu and then reduced to nitrite by electron from Cu<sup>0</sup>, resulting in the formation of Cu<sup>1</sup> (Eq. (2)). Fig.10b presented the Pd 3d spectra of cathode before and after reduction. It showed that two peaks at 335.2 and 340.5 eV were observed before reduction; after that, the two peaks (335.1 and 340.4 eV) were also detected. This indicated that Pd<sup>0</sup> did not change in the nitrate reduction. It is consistent with previous studies that Pd does not present activity for nitrate reduction, but is effective for nitrite reduction [26]. Therefore, nitrite can be easily adsorbed and converted into N<sub>2</sub> or ammonium via active hydrogen adsorbed on the Pd surface (Eqs. (3)–(4)) [51]. In addition, the activated H cannot only reduce nitrite to N<sub>2</sub>, but also rejuvenates Cu<sup>1</sup> to Cu<sup>0</sup> (Eq. (5)).



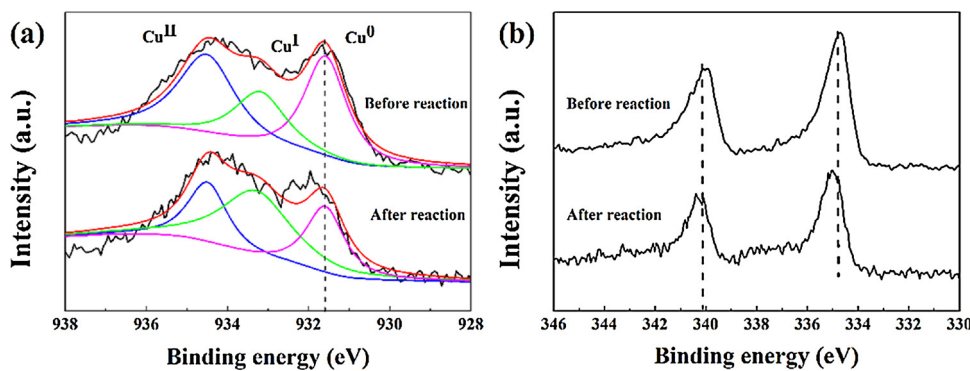
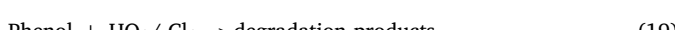
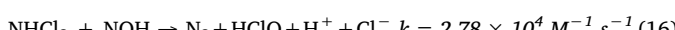
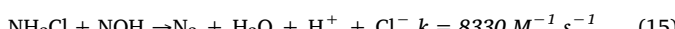
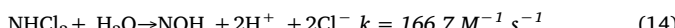
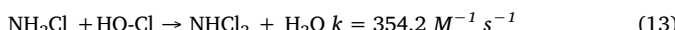
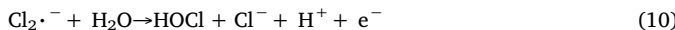


Fig. 10. XPS spectra for the narrow scan of (a) Cu 2p and (b) Pd 3d on the Pd – Cu/NF cathode surface before and after reaction.



### 3.5. Mechanism of NH<sub>4</sub><sup>+</sup>-N and phenol oxidation on photoanode

Phenol and ammonium-N were oxidized at photoanode area. Under irradiation, the photogenerated hole yield at WO<sub>3</sub> can convert water to hydroxyl radical and chlorine ion to chlorine radical, respectively (Eqs. (6)–(8)). Cl· could be quenched by Cl<sup>−</sup> to form Cl<sub>2</sub>·<sup>−</sup> and then hydrolyzed to HClO in Eqs. (9)–(10). The Cl· dominated the oxidation of NH<sub>4</sub><sup>+</sup>-N owing to its high selectivity with the electron-rich compound (Eqs. (11)–(16)). HOCl formed could participate in the degradation of NH<sub>4</sub><sup>+</sup>-N species [49]. Indeed, the transformation from NH<sub>4</sub><sup>+</sup> to N<sub>2</sub> was controlled by the ratio of Eqs. (13) and (14). Certain amounts of nitrate were formed during the process (Eqs. (17)–(18)). However, the produced NO<sub>3</sub><sup>−</sup>-N was converted to N<sub>2</sub> on Pd-Cu/NF, realizing complete removal of TN. Phenol was oxidized to intermediate products or CO<sub>2</sub> by OH· for improving TOC removal. At the same time, Cl· can enhance the organic degradation (Eq. (19)).



### 3.6. Recycling performance

Electricity production was evaluated by measuring the output power density of WFC system in Fig.11a and the results were presented in Table 1. The oxidation of organic matter is the exothermic process, which indicates that the chemical energy of organics in wastewater can

be converted into electric current [52]. Pure electrolyte without organics presented the small P<sub>max</sub> (0.75 mW cm<sup>−2</sup>) and this part of energy was converted from the sunlight by Si PVC. Fill factor (FF) was then calculated by the following equation.

$$P_{\text{max}} = \text{FF} \times J_{\text{SC}} \times V_{\text{OC}} \quad (20)$$

Where P<sub>max</sub> is the maximum power density. J<sub>sc</sub> and V<sub>oc</sub> are short-circuit current density and open-circuit voltage, respectively. As expected, the addition of phenol resulted in the production of much higher photocurrents compared to the organic-free electrolyte. The maximum output power density 1.23 mW cm<sup>−2</sup> and the FF was 0.29 (Table 1). The power improvement (0.48 mW cm<sup>−2</sup>) was attributed to the degradation of phenol through WFC process to generate electrical energy.

Fig.11b showed the cycling stability of Pd-Cu/NF cathode in the continuous treatment of solution containing 30 mg L<sup>−1</sup> nitrate-N and 20 mg L<sup>−1</sup> phenol. The removal of TN and TOC were nearly remained the same as fresh sample after five successive cycles (94.1% and 53.5%), which indicated that Pd-Cu/NF cathode was stable. Furthermore, the XRD diffraction patterns of the used Pb-Cu/NF cathode were found to be similar to that recorded before reaction (Fig.S12). The results demonstrated that the fabricated WFC system possessed good stability, which had a potential for long-term application.

### 4. Conclusion

This work reported a novel method to achieve efficient removal of TOC and TN with simultaneous electricity generation of nitrogen-containing organic wastewater. Organic and ammonium-N were transformed into CO<sub>2</sub> and N<sub>2</sub> by hydroxyl and chlorine radicals, respectively, while generating electricity at the same time in a self-bias wastewater fuel cell. The nitrate-N was finally converted to N<sub>2</sub> on Pd-Cu modified Ni foam cathode with high selectivity, realizing the complete removal of nitrogen from the water. Employing series-connected WO<sub>3</sub> electrodes and silicon photovoltaic cells as a hybrid photoanode, the system succeeded in both generating photovoltage and extending the light harvesting due to their complementary absorption of solar light. Results indicated the removal efficiency of nitrate-N and ammonium-N within 90 min was 98.7% and 91.5%, respectfully, and nitrogen was completely transformed to nitrogen gas by extending reaction time to 120 min. The system also showed a superior performance for phenol degradation with a maximum removal rate of 99.1% in 90 min. Combined with the analysis of ESR and free radical capture experiment, it was concluded that Cl· played an important role in ammonia-N oxidation. The output power density of the system is up to 1.23 mW cm<sup>−2</sup>. This WFC system offers a self-sustaining, energy-saving method for simultaneous nitrogen and organic matter treatment and energy recovery.

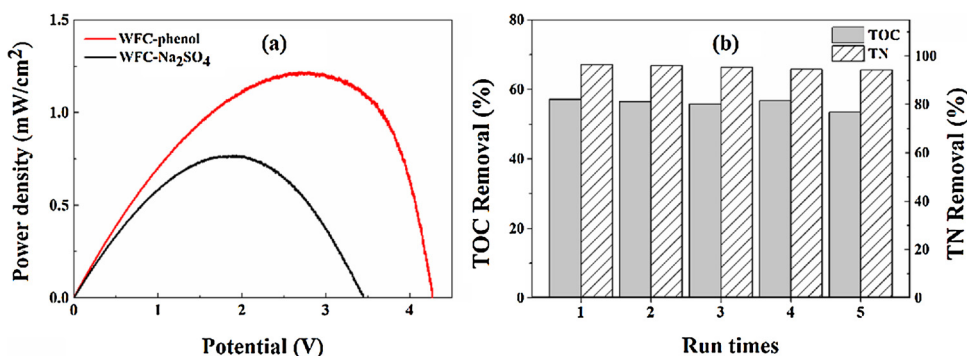


**Fig. 11.** (a) I-V characteristic curve and power density curve of the self-biased WFC system. (b) TOC and TN removal efficiency in system during five tests at 90 min intervals. The initial conditions, NaCl 0.05 M, pH = 5, nitrate-N 30 mg L<sup>-1</sup> and phenol 20 mg L<sup>-1</sup>.

**Table 1**

System current-voltage characteristics of the WFC system using various compounds at pH 5.0.

Compounds	Voc (V)	J <sub>sc</sub> (mA cm <sup>-2</sup> )	P <sub>max</sub> (mWcm <sup>-2</sup> )	FF
Na <sub>2</sub> SO <sub>4</sub> (0.05 M)	3.44	0.74	0.75	0.30
Phenol (20 mg L <sup>-1</sup> )	4.23	1.01	1.23	0.29

## Acknowledgments

The authors would like to acknowledge the National Natural Science Foundation of China (No. 21776177, 51578332, 21576162) and SJTU-AEMD for support.

## Appendix A. Supplementary data

Supplementary material related to this article can be found, in the online version, at doi:<https://doi.org/10.1016/j.apcatb.2018.07.036>.

## References

- [1] H. Shin, S. Jung, S. Bae, W. Lee, H. Kim, Environ. Sci. Technol. 48 (2014) 12768–12774.
- [2] G. Liu, S. You, Y. Tan, N. Ren, Environ. Sci. Technol. 51 (2017) 2339–2346.
- [3] X. Yang, S. Wang, L. Zhou, Bioresour. Technol. 104 (2012) 65–72.
- [4] E.T. Lim, G.T. Jeong, S.H. Bhang, S.H. Park, D.H. Park, Bioresour. Technol. 100 (2009) 6149–6154.
- [5] Y. Wang, Y. Peng, T. Stephenson, Bioresour. Technol. 100 (2009) 3506–3512.
- [6] M.L. Bosko, M.A.S. Rodrigues, J.Z. Ferreira, E.E. Miró, A.M. Bernardes, J. Membr. Sci. 451 (2014) 276–284.
- [7] J. Kim, M.M. Benjamin, Water Res. 38 (2004) 2053–2062.
- [8] Y. Zeng, H. Walker, Q. Zhu, J. Hazard. Mater. 324 (2017) 605–616.
- [9] T. Öznüller, B. Özdurak, H. ÖzTÜRK Doğan, J. Electroanal. Chem. 699 (2013) 1–5.
- [10] J.T. Jasper, O.S. Shafaat, M.R. Hoffmann, Environ. Sci. Technol. 50 (2016) 10198–10208.
- [11] H. Wang, X. Zhang, Y. Su, H. Yu, S. Chen, X. Quan, F. Yang, Appl. Surf. Sci. 311 (2014) 851–857.
- [12] D. Wang, Y. Li, G. Li Puma, C. Wang, P. Wang, W. Zhang, Q. Wang, Appl. Catal. B: Environ. 168–169 (2015) 25–32.
- [13] W.-W. Li, H.-Q. Yu, Z. He, Energy Environ. Sci. 7 (2013) 911–924.
- [14] B.E. Logan, B. Hamelers, R. Rozendal, U. Schröder, J. Keller, S. Freguia, P. Aelterman, W. Verstraete, K. Rabaey, Environ. Sci. Technol. 40 (2006) 5181–5192.
- [15] B. Min, J. Kim, S. Oh, J.M. Regan, B.E. Logan, Water Res. 39 (2005) 4961–4968.
- [16] Y. Liu, J. Li, B. Zhou, X. Li, H. Chen, Q. Chen, Z. Wang, L. Li, J. Wang, W. Cai, Water Res. 45 (2011) 3991–3998.
- [17] P. Lianos, J. Hazard. Mater. 185 (2011) 575–590.
- [18] Z. Zhou, Z. Wu, Q. Xu, G. Zhao, J. Mater. Chem. A 5 (2017) 25450–25459.
- [19] X. Li, J. Li, J. Bai, Y. Dong, L. Li, B. Zhou, Nano-Micro Lett. 8 (2016) 221–231.
- [20] Y. Zhang, B. Tang, Z. Wu, H. Shi, Y. Zhang, G. Zhao, Green Chem. 18 (2016) 2424–2434.
- [21] Z. Wu, J. Wang, Z. Zhou, G. Zhao, J. Mater. Chem. A 5 (2017) 12407–12415.
- [22] R. Wang, J. Bai, Y. Li, Q. Zeng, J. Li, B. Zhou, Nano-Micro Lett. 9 (2016).
- [23] C. Feng, L. Huang, H. Yu, X. Yi, C. Wei, Water Res. 76 (2015) 160–170.
- [24] W.L. Wang, Q.Y. Wu, N. Huang, T. Wang, H.Y. Hu, Water Res. 98 (2016) 190–198.
- [25] Y. Xiang, J. Fang, C. Shang, Water Res. 90 (2016) 301–308.
- [26] S. Jung, S. Bae, W. Lee, Environ. Sci. Technol. 48 (2014) 9651–9658.
- [27] G.W. Yang, C.L. Xu, H.L. Li, Chem. Commun. (Camb) (2008) 6537–6539.
- [28] C. Battaglia, A. Cuevas, S. De Wolf, Energy Environ. Sci. 9 (2016) 1552–1576.
- [29] Q. Zeng, J. Bai, J. Li, B. Zhou, Y. Sun, Nano Energy 41 (2017) 225–232.
- [30] M.S. Prévôt, K. Sivula, J. Phys. Chem. C 117 (2013) 17879–17893.
- [31] S.S. Kalanur, Y.J. Hwang, S.Y. Chae, O.S. Joo, J. Mater. Chem. A 1 (2013).
- [32] Y. Zhang, J. Li, J. Bai, Z. Shen, L. Li, L. Xia, S. Chen, B. Zhou, Environ. Sci. Technol. 52 (2018) 1413–1420.
- [33] Q. Zeng, J. Li, J. Bai, X. Li, L. Xia, B. Zhou, Appl. Catal. B: Environ. 202 (2017) 388–396.
- [34] Q. Peng, H. Zhao, L. Qian, Y. Wang, G. Zhao, Appl. Catal. B: Environ. 174–175 (2015) 157–166.
- [35] J. Fang, Y. Fu, C. Shang, Environ. Sci. Technol. 48 (2014) 1859–1868.
- [36] J. Li, W. Xu, J. Luo, D. Zhou, D. Zhang, L. Wei, P. Xu, D. Yuan, Nano-Micro Lett. (2017) 10.
- [37] Y. Yoshinaga, T. Akita, I. Mikami, T. Okuhara, J. Catal. 207 (2002) 37–45.
- [38] Q.-S. Chen, Z.-N. Xu, S.-Y. Peng, Y.-M. Chen, D.-M. Lv, Z.-Q. Wang, J. Sun, G.-C. Guo, J. Power Sour. 282 (2015) 471–478.
- [39] H. Zhao, L. Qian, X. Guan, D. Wu, G. Zhao, Environ. Sci. Technol. 50 (2016) 5225–5233.
- [40] L. Su, K. Li, H. Zhang, M. Fan, D. Ying, T. Sun, Y. Wang, J. Jia, Water Res. 120 (2017) 1–11.
- [41] J. Ding, W. Li, Q.-L. Zhao, K. Wang, Z. Zheng, Y.-Z. Gao, Chem. Eng. J. 271 (2015) 252–259.
- [42] A. Ansón, E. Lafuente, E. Urriolabeitia, R. Navarro, A.M. Benito, W.K. Maser, M.T. Martínez, J. Phys. Chem. B. 110 (2006) 6643–6648.
- [43] S.-E. Bae, K.L. Stewart, A.A. Gewirth, J. Am. Chem. Soc. 129 (2007) 10171–10180.
- [44] X. Huang, Q. Shen, J. Liu, N. Yang, G. Zhao, Energy Environ. Sci. 9 (2016) 3161–3171.
- [45] X. Zhang, W. Li, E.R. Blatchley 3rd, X. Wang, P. Ren, Water Res. 68 (2015) 804–811.
- [46] Y. Yang, J. Shin, J.T. Jasper, M.R. Hoffmann, Environ. Sci. Technol. 50 (2016) 8780–8787.
- [47] H. Park, C.D. Vecitis, M.R. Hoffmann, J. Phys. Chem. C. 113 (2009) 7935–7945.
- [48] M.J. Watts, K.G. Linden, Water Res. 41 (2007) 2871–2878.
- [49] S. Xiao, J. Qu, X. Zhao, H. Liu, D. Wan, Water Res. 43 (2009) 1432–1440.
- [50] T. Li, Y. Jiang, X. An, H. Liu, C. Hu, J. Qu, Water Res. 102 (2016) 421–427.
- [51] J. Shi, C. Long, A. Li, Chem. Eng. J. 286 (2016) 408–415.
- [52] Y. Liu, J. Li, B. Zhou, X. Li, H. Chen, Q. Chen, Z. Wang, L. Li, J. Wang, W. Cai, Water Res. 45 (2011) 3991–3998.